Feasibility Study on Joining Aluminum Tube with Alumina Ceramic Rod Using Magnetic Pulse Crimping Process

U. Singh*, A. Rajak
Department of Mechanical Engineering, Indian Institute of Technology, Indore 453552, India
*Corresponding author. Email: phd2201103006@iiti.ac.in

Abstract

Ceramic-metal joints play a vital role in structural applications, offering benefits such as strength, lightweight, high strength-to-weight ratio, corrosion resistance, and high-temperature performance. These joints are widely used in fields ranging from electronics and biomedical devices to aerospace and automotive industries. However, joining ceramics and metals is challenging due to differences in atomic bonding and thermal expansion properties. Traditional methods, such as brazing, friction welding, and fusion welding, often induce thermal stresses and residual strain, leading to defects like cracks and intermetallic formation at the joint interface. Magnetic Pulse Crimping (MPC) is an environmentally friendly, quick, and cold solid-state material joining process that does not create heat-affected zones and mitigates these issues. This study uses the MPC process to investigate the feasibility of joining an AA 1050 aluminum alloy tube with an alumina ceramic rod. The experiments were performed at various discharge energies using an Archimedean spiral coil and a step taper field shaper to evaluate the joint's strength and metal-ceramic interface behavior. Non-sinusoidal waviness patterns have been observed at the metal-ceramic joint interface. The numerical analysis used the LS DYNA EM module to measure the current density, magnetic field, Von Mises stresses, and impact velocity on the flyer tube. The manuscript contributes to the understanding of ceramic-metal joining under electromagnetic forming conditions.

Keywords

Magnetic Pulse Crimping, Archimedean spiral coil, AA 1050, Alumina, Ceramic-metal joints.

1 Introduction

Ceramics and metal joints are becoming crucial in structural applications due to their functional requirements, such as strength, lightweight, high strength-to-weight ratio, corrosion resistance, and high-temperature performance (Lemus-Ruiz et al. 2011). These joints are used widely in vacuum tubes, electronics, insulators, sapphire-metal windows, biomedical devices, and rocket igniter bodies (Loehman and Loehman 2009). Ceramic components of an automobile engine are joined with metal using the brazing technique for strength, resistance to fatigue, creep, and oxidation. High pressure and temperature bond ceramic with metal, and a brittle intermetallic is formed at the interface due to differential cooling rate and mechanical response (Jadoon 2004; Palit and Meier 2006). Joining ceramics with metals is challenging due to differences in atomic bond configurations and properties, as ceramics have ionic and covalent bonds with stable peripheral electrons, making them resistant to fusion welding-assisted joining methods (Zhou 2008).

Diffusion bonding is one of the popular solid-state joining techniques used to join metal with ceramic by applying pressure at elevated temperatures and controlling the interface's microstructure. This method provides joint strength equal to the base metal with reduced defects, reduced cracking, and relaxed thermal residual stress, but it takes more joining time and high equipment due to vacuum conditions (Akselsen 1992). The difference in thermo-mechanical properties of aluminum alloy and ceramic due to their metal-ceramic nature makes the MPC more favorable, as it is a cold metal-forming process (Yao et al., 2023).

This manuscript presents a feasibility study on joining AA 1050 with ceramic rods using a magnetic pulse crimping process. Experiments were performed at various discharge energies using an Archimedean spiral (AS) coil and a step taper field shaper. A cross-sectional study of the sample has been conducted to understand the metal-ceramic joint interface.

2 Experimental procedure:

Joining was performed between a 1 mm-thick AA 1050 flyer tube and an 8 mm diameter alumina target rod with a 1 mm standoff distance for optimal results. To improve the bonding and joining efficacy, the contacting surface of the flyer and target was made coarse using 80-grit size polishing paper by increasing the surface energy.

Experiments were performed using a magnetic pulse forming machine with a maximum discharge energy capacity of 10 kJ, maximum voltage of 15 kV, capacitance of 100 μF, circuit resistance of 22 mΩ, and circuit inductance of 2 μH. In the Archimedean spiral coil, the radial distance between the consecutive turns remains constant, which provides strength and durability to the forming coil. The AA 1050 flyer tube was placed over the alumina rod in the field shaper and the primary coil vicinity. The flyer tube and target rod were fixed from the non-crimping ends to remain equidistant, maintaining a 1 mm constant standoff distance. Fig. 1 (a) and (b) show the arrangement's isometric and front-half sectional views. Fig. 1. (c) and (d) show the detailed coil and field shaper dimensions. Experiments were

performed at different discharge energy capacities from 1 kJ to 6 kJ to optimize the MPC process.

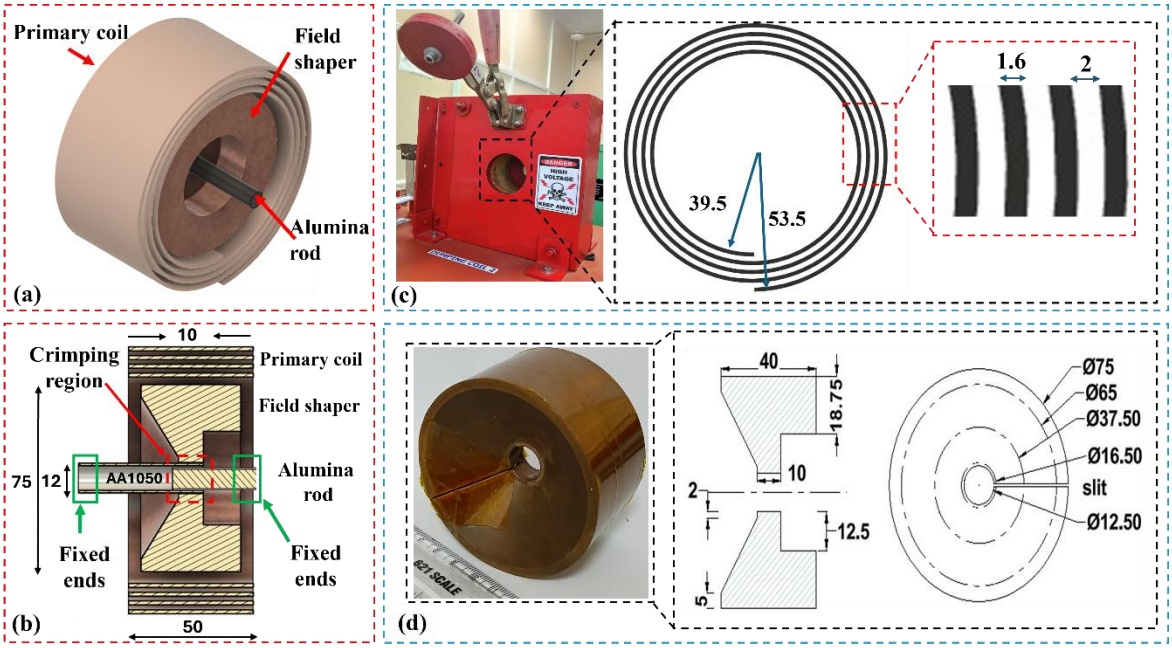

Figure 1. *(a) Isometric, (b) front half sectional view of the arrangement, (c) Coil, and (d) Field shaper with detailed dimensions in mm.*

3 Numerical study:

The coupled numerical simulations were performed using the LS-DYNA Electromagnetics (EM) module. The EM module solves electromagnetics and structural coupled simulations with Finite Element Method (FEM) – Boundary Element Method (BEM) methods with eddy current solvers. Johnson-Cook's model defines the plastic behavior of the materials and the parameters in Table 1, Eq. 1 and Eq. 2 (R. Johnson and H. Cook 1983).

$$\sigma = (A + B \in^n)\left(1 + C \ ln \dot{\in}_p\right)(1 - T^m) \quad (1)$$

$$T = \frac{T_i - T_{ambient}}{T_{melt} - T_{ambient}} \quad (2)$$

Where σ is equivalent true stress, ε is true strain; A, B, C, n, and m are material-dependent parameters in which A is the yield strength, B and n represent the strain hardening effect values, C is the strain rate sensitivity constant, whereas m is a thermal softening exponent. $\in^n$ indicates equivalent plastic strain, $\dot{\in}_p$ is a plastic strain rate. T_i, $T_{ambiemt}$ and T_{melt} are instant, ambient, and melting point temperatures of AA1050.

Material	A (MPa)	B (MPa)	C	n	T (K)
AA1050 tube	110	150	0.01	0.4	293
Copper FS	90	292	0.025	0.31	293

Table 1. *Johnson-Cook parameters for AA1050 tube and copper.*

Ceramics subjected to impact load respond according to the flyer material, contact area, velocity, and mechanical characteristics (Cronin et al. 2003). Johnson-Holmquist's (JH-2) ceramic constitutive model for alumina describes brittle materials' response under large deformations, as mentioned in Eq. 3. The effective normalized strength (σ^*) combines intact (σ_i^*) and fractured (σ_f^*) material states via a damage parameter (D) :

$$\sigma^* = \sigma_i^* - D\left(\sigma_i^* - \sigma_f^*\right) \tag{3}$$

Intact strength (σ_i^*):

$$\sigma_i^* = A(P^* + T^*)^N(1 + C\ln\ \dot{\varepsilon}^*) \tag{4}$$

Fractured strength $\left(\sigma_f^*\right)$:

$$\sigma_f^* = B(P^*)^M(1 + Cln\ \dot{\varepsilon}^*) \tag{5}$$

Where $P^* = P/P_{\mathrm{HEL}}$ (pressure normalized by Hugoniot Elastic Limit pressure), and $\dot{\varepsilon}^* = \dot{\varepsilon}/\dot{\varepsilon}_0$ (strain rate normalized by a reference rate).

Further, the equation of state (Pressure-Volume relationship):

$P = K_1\mu + K_2\mu^2 + K_3\mu^3 + \Delta P$ ($for\ compression,\ \mu = \rho/\rho_0 - 1 \geq 0$) (6)

Where, K_1, K_2, K_3 is material-specific bulk modulus coefficients, and ΔP is the bulking pressure due to damage.

The Johnson-Holmquist ceramic constitutive model for alumina is mentioned in Table 2.

Strength constants	A	B	C	M	N
	0.93	0.31	0	0.60	0.60
	EPSI	Tensile strength (GPa)	SFMAX	HEL (GPA)	PHEL (GPA)
	1.00	0.2	0.0	2.79	1.46
Damage constants	D1	D2			
	0.005	1.0			
Equation of state	K1 (GPa)	K2 (GPa)	K3 (GPa)	BETA	
	130.95	0.0	0.0	1.0	

Table 2. *Johnson- Holmquist ceramic constitutive model for Alumina.*

Hexahedron elements provide accuracy, stability in handling extreme deformations, and better convergence behavior in nonlinear simulations. The mesh size was selected for optimal accuracy and cost of the solution. The total number of elements for the AS coil, step-

tapered FS, flyer tube, and target rod was 40950, 18876, 1392, and 1627, respectively. The mesh size of all parts and the element selected for the study is shown in Fig. 2.

The coil was selected as a rigid body, whereas J-C plasticity material properties were assigned to the FS and flyer to study the deformation, as in equation 1. Johnson-Holmquist (J-H) ceramic constitutive models have been selected to illustrate the response of brittle alumina under significant deformations.

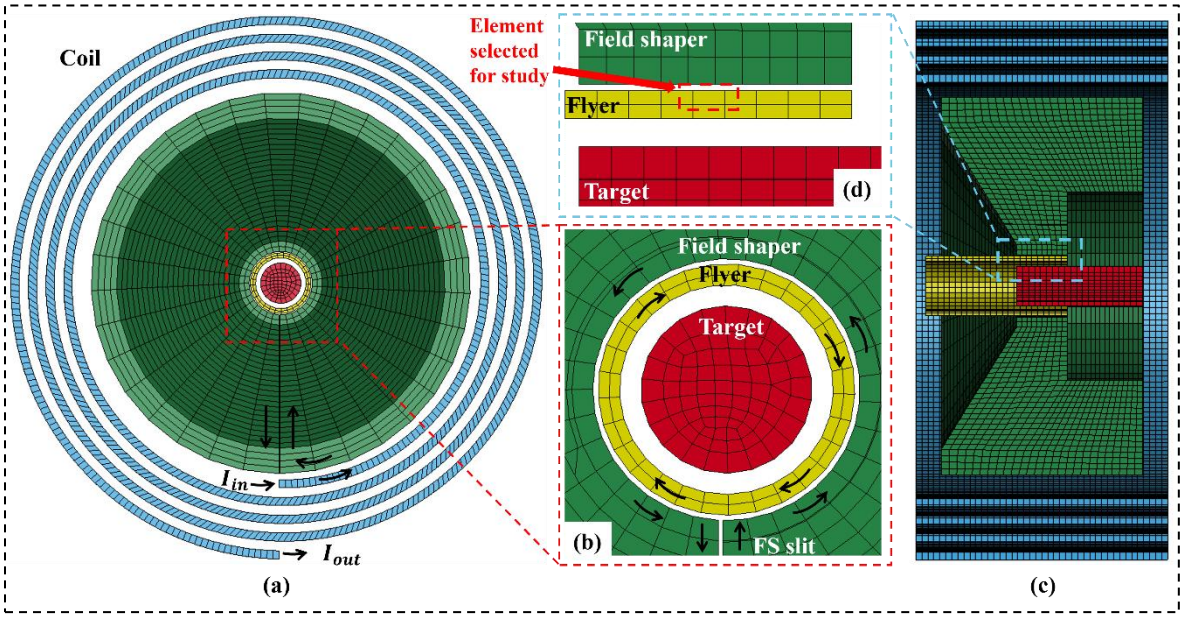

Figure 2. *Meshing on the parts and element selection for the study.*

4 Results and discussion:

Figure 3 (a) depicts the radial view and (b) longitudinal view along with fractured parts of the ceramic rod of the metal-ceramic samples. From the experiments, it can be concluded that the proper joining was achieved at 4 kJ energy. Below 4 kJ, the AA 1050 tube had insufficient deformation and an improper joint with the rod. For more than 5 kJ, a brittle fracture of the ceramic rod at the non-crimping zone and crushing was observed. The joint quality was assessed using visual inspection and mechanical integrity of the sample. Samples with no visible joint were considered poor, whereas samples with localized interface contact without complete continuity were considered improper, and the defect-free sample with proper contact in the crimping region was termed a proper joint. Improper joining was evident at an energy less than 4 kJ, the proper joint was achieved at 4 kJ, and the brittle fracture of the ceramic rod was observed for discharge energy of more than 5 kJ.

On the other hand, alumina crushing was prevalent at 6 kJ discharge energy. The observations are mentioned in Table 3. The deformation of the AA 1050 tube was assessed based on post-test radial and longitudinal measurements and visual inspection of the flyer tube geometry compared to its original dimensions.

S. No	Discharge energies (kJ)	Discharge voltage (kV)	Effect on the sample

1	1.0	4.50	No joining at the interface
2	2.0	6.45	Improper joint at the interface
3	3.0	7.80	Improper joint at the interface
4	4.0	9.00	Proper joint at the interface
5	5.0	10.05	Fracture of alumina rod
6	6.0	10.95	Crushing of alumina rod

***Table 3**. Discharge energy optimization for joining.*

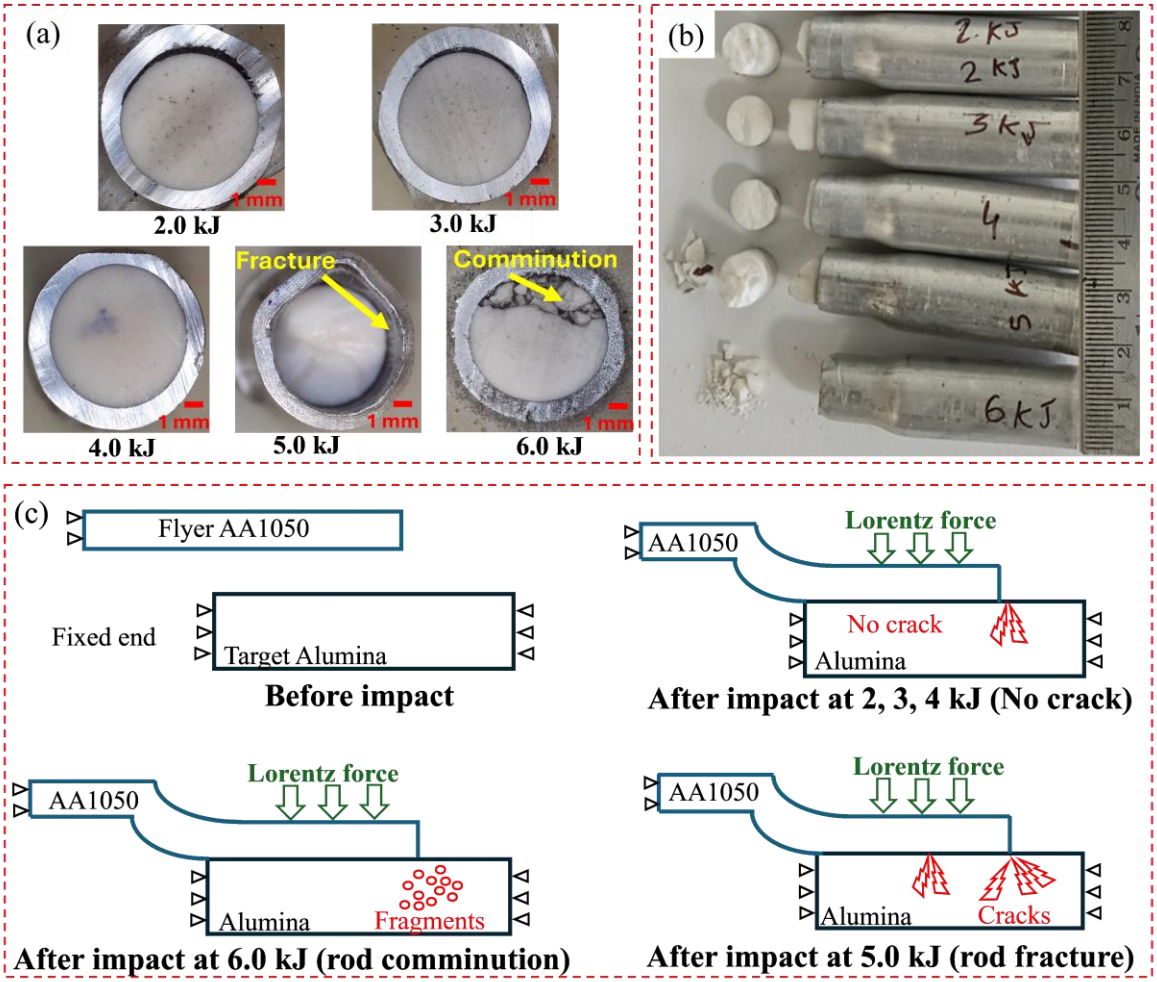

***Figure 3.** (a) Radial and (b) longitudinal view of joined ceramic metal samples, and (c) fracture and fragment generation in alumina rod.*

During the MPC, the rapidly induced Lorentz forces cause a high-velocity impact of the flyer on the target, generating a compressive stress wave at the ductile-brittle joint interface. The geometry of the crimping joint, particularly near the crimping region, causes abrupt material transition, and edge discontinuities lead to localized stress amplification. At energy levels higher than 4.0 kJ, the compressive stress wave surpasses the local dynamic strength of the target, initiating crack formation. At higher energies of 5 and 6 kJ, the resulting fracture front propagates at the elastic wave speed of the alumina. It forms a conoid of comminuted or pulverized alumina at the impact location. When the compressive stress wave reaches the

free surface, it is reflected as a tensile wave, causing spallation or tensile cracking (Kaufmann et al. 2003).

4.1 Cross-sectional analysis:

After choosing the suitable discharge energy by trial and error, the remaining experiments were performed at 4 kJ to investigate the metal-ceramic joint interface. Fig. 4 (a) shows a cross-sectional view of a ceramic metal joint at 4 kJ, where the uniform joining of the AA1050 flyer with an alumina target is visible. Fig. 4 (b) shows the metal penetration into the ceramic with a 71-micron width, and Figs. 4 (c) and (d) show the same ceramic metal joint interface at 200X and 500X magnification, depicting irregular wavy interaction. The material hardness difference causes this irregular, non-sinusoidal wavy pattern at the interface.

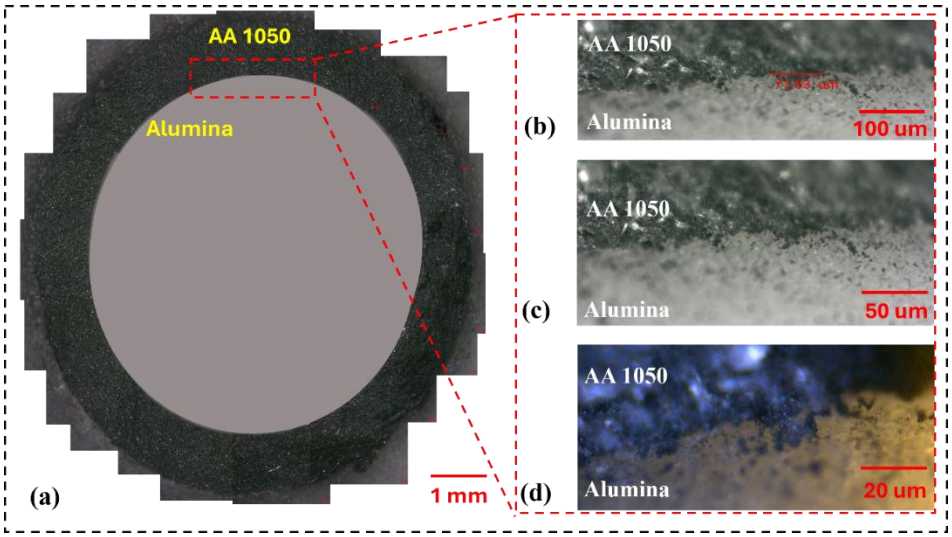

Figure 4. *(a) Cross-sectional view of the ceramic metal joint at 4 kJ, (b) Interface at 100X, (c) 200X, and (d) 500X magnification.*

A complex stress field develops when the aluminum flyer impacts the ceramic at high velocity. The brittle ceramic accumulates damage when local stresses exceed its dynamic strength. The compressive-induced damage and bulking (volume increase due to fracturing) cause surface distortion and irregularities near the impact zone. This transition between compressive and tensile states and evolving damage at the crimping interface generates uneven localized expansion. Additionally, fractured ceramic material tends to bulk and lose structural coherence. When confined or partially constrained by the aluminum flyer, this expansion may not occur uniformly, especially along edges and corners where geometric effects amplify stress. This asymmetry results in the wavy interface as the damaged ceramic attempts to accommodate internal stress redistribution. Therefore, irregular waviness is the physical expression of stress wave interactions, localized damage accumulation, and inhomogeneous bulking, as discussed by (Reijer 1991).

5 Simulation Results: current density, magnetic field, Von Mises stress, and Impact velocity on the flyer tube

From the experimental analysis, the samples joined at 4 kJ gave an optimal interface. Further simulations were performed at 4 kJ discharge energy to understand the current density, magnetic field, Lorentz force, and impact velocity on the flyer tube during crimping. The element on the outer flyer tube surface, located opposite the FS slit, has been selected to study the behavior of the flyer tube. Values of current density taken during the impact at 29 µs are 13.44 kA/mm^{2,} and at 41 µs corresponding to the highest value of discharge current are 9.96 kA/mm^2, as mentioned in Fig. 5 (a) and (b) Whereas, Fig. 5 (c) and (d) shows the magnetic field density is 10.97 Tesla and 10.81 Tesla at 29 µs and 41 µs, respectively.

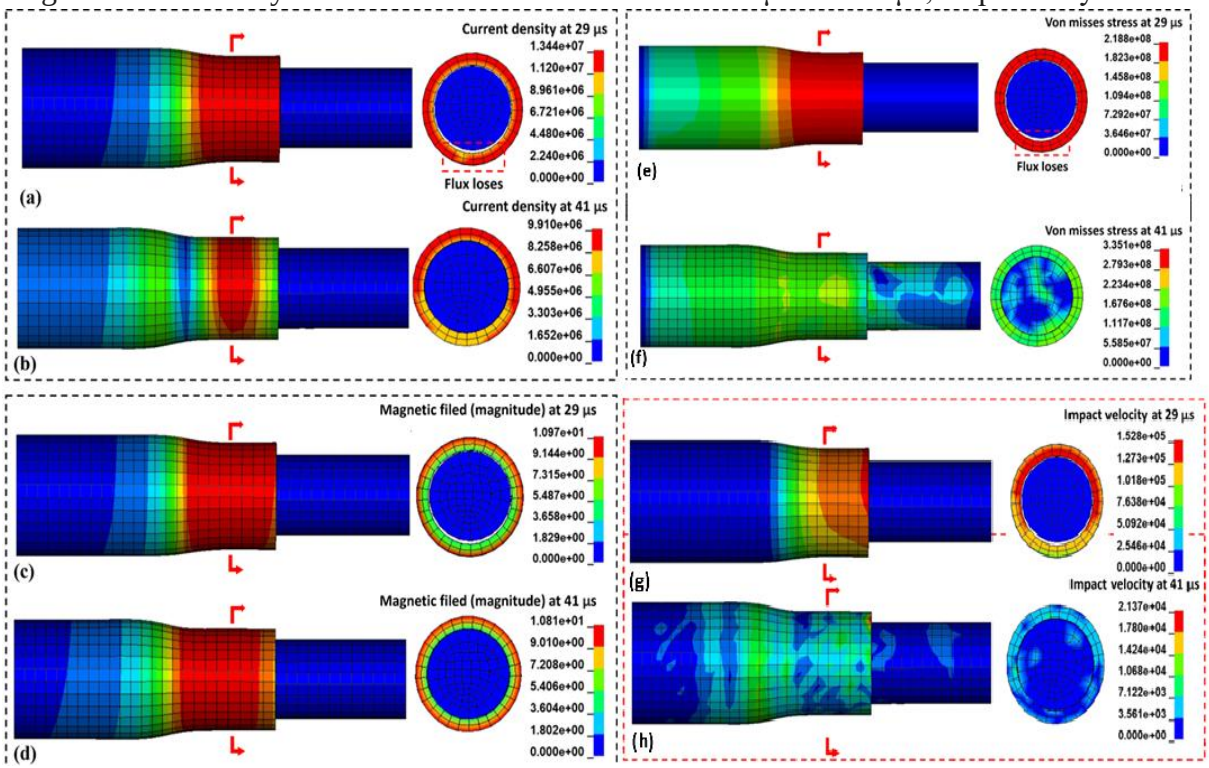

Figure 5. *Contours for current density on the flyer at (a) 29 µs, (b) 41 µs, and magnetic field at (c) 29 µs, (d) 41 µs and Von Mises stresses on the flyer at (e) 29 µs, and (f) 41 µs, and Impact velocity at (g) 29 µs, and (h) 41 µs.*

The current density and magnetic field are maximum in the center of the crimping zone and decrease with distance. Uneven deformation and flux losses take place due to the FS slit area, which is shown in the inset view of Fig 5. (a). The Lorentz force induces a complex stress state in the flyer tube. Von Mises stress calculations indicate that plastic deformation initiates at 219 MPa after 29 µs, as shown in Fig. 5(e). A subsequent reduction in stress is observed during the peak magnetic field, as seen in Fig. 5(f). The highest flyer impact velocity of 152.8 m/s was observed before the impact at 29 µs. In contrast, the sudden drop in velocity occurs after the impact and becomes negligible, as mentioned in Fig. 5 (g) and (h).

6 Conclusions:

This study investigates the feasibility of joining AA 1050 aluminum with a ceramic rod using magnetic pulse crimping. The experiments were performed at various discharge energies from 1.0 kJ to 6.0 kJ, using an Archimedean spiral coil and a step taper field shaper to evaluate the joint's strength and interface behavior. The optimum cross-section was achieved at 4 kJ discharge energy. A non-sinusoidal wavy pattern with 71-micron thickness has been observed at the joint interface for the 4 kJ sample. The fracture of the alumina rod has been observed due to compressive stresses and high-velocity impacts, which have been mitigated by optimizing the discharge energy.

Numerical analysis of parameters such as current density, magnetic field, Lorentz force, and impact velocity indicates that the most significant deformation occurs at the flyer tube side because the FS concentrates and amplifies the magnetic field. The flyer tube's highest current density, magnetic field, Von Mises, and impact velocity values are 13.44 kA/mm^2, 10.9 T, 210 MPa, and 152 m/s, respectively. The results contribute to the understanding of ceramic-metal joining under electromagnetic forming conditions.

References

Akselsen, O. M. 1992. "Diffusion Bonding of Ceramics." *Journal of Materials Science* 27 (3): 569–79. https://doi.org/10.1007/BF00554019.

Cronin, Duane S., Khanh Bui, Christian Kaufmann, Grant McIntosh, and Todd Berstad. 2003. "Implementation and Validation of the Johnson-Holmquist Ceramic Material Model in LS-Dyna." In *4th European LS-DYNA Users Conference*, Material I:47–59. D–I. Germany: DYNAmore GmbH.

Jadoon, A. K. 2004. "Employing Reactive Synthesis for Metal to Ceramic Joining for High Temperature Applications." *Journal of Materials Science* 39 (2): 593–604. https://doi.org/10.1023/B:JMSC.0000011516.43086.20.

Kaufmann, Christian, Duane Cronin, Michael Worswick, Gilles Pageau, and Andre Beth. 2003. "Influence of Material Properties on the Ballistic Performance of Ceramics for Personal Body Armour." *Shock and Vibration* 10 (1): 51–58. https://doi.org/10.1155/2003/357637.

Lemus-Ruiz, Jose, Leonel Ceja-Cardenas, Egberto Bedolla-Becerril, and Victor H. 2011. "Production, Characterization, and Mechanical Evaluation of Dissimilar Metal/Ceramic Joints." In *Nanocomposites with Unique Properties and Applications in Medicine and Industry*, edited by John Cuppoletti. InTech. https://doi.org/10.5772/21720.

Loehman, Ronald E., and Ronald Loehman. 2009. *Characterization of Ceramics*. Momentum Press.

Palit, D., and A. M. Meier. 2006. "Reaction Kinetics and Mechanical Properties in the Reactive Brazing of Copper to Aluminum Nitride." *Journal of Materials Science* 41 (21): 7197–7209. https://doi.org/10.1007/s10853-006-0920-z.

R. Johnson, Gordon, and William H. Cook. 1983. "A Constitutive Model And Data For Metals Subjected To Large Strains, High Strain Rates And High Temperatures." *Proceedings of the 7th International Symposium on Ballistics*.

Reijer, Paulus Cornelis Den. 1991. "Impact on Ceramic Faced Armour." PhD thesis, Delft, Netherlands: TU Delft University, Netherlands. TU Delft Institutional Repository. https://resolver.tudelft.nl/uuid:25ffb34c-adb4-4e17-a294-6b707ddc0e9b.

Yao, Yuanheng, Ao Chen, Dayong Wang, Shaoluo Wang, Hao Jiang, Guangyao Li, and Junjia Cui. 2023. "Fatigue Behavior of Al-CFRP Spot-Welded Joints Prepared by Electromagnetic Pulse Welding." *International Journal of Fatigue* 174 (September):107715. https://doi.org/10.1016/j.ijfatigue.2023.107715.

Zhou, Y. 2008. *Microjoining and Nanojoining*. Woodhead Publishing Limited. https://doi.org/10.1533/9781845694043.